Int. J. Heat Mass Transfer. Vol. 18, pp. 849–862. Pergamon Press 1975. Printed in Great Britain

LAMINAR FLOW FRICTION AND FORCED CONVECTION HEAT TRANSFER IN DUCTS OF ARBITRARY GEOMETRY

R. K. SHAH
Harrison Radiator Division, General Motors Corporation, Lockport, NY 14094, U.S.A.

(*Received* 25 *June* 1974 *and in revised form* 9 *September* 1974)

Abstract—A least-squares-matching technique is presented to analyze fully developed laminar fluid flow and heat transfer in ducts of arbitrary cross-section. Forced convection heat transfer is considered under constant axial heat-transfer rate with arbitrary peripheral thermal boundary conditions. As an application of the method, flow and heat-transfer results are presented for the duct geometries of isosceles triangular, rounded corner equilateral triangular, sine, rhombic and trapezoidal cross-sections. These numerical results are discussed from a heat exchanger designer's viewpoint.

NOMENCLATURE

$\mathbf{A}$, $m \times n$ matrix;
A_c, duct cross-sectional (flow) area;
a, b, c, dimensions as specified in Fig. 1;
c_1, a constant (pressure gradient parameter);
c_p, specific heat of fluid at constant pressure;
D_h, hydraulic diameter, $4A_c/P$;
E, fluid pumping power defined by equation (54);
f, Fanning friction factor for fully developed laminar flow [dimensionless];
g_c, proportionality factor in Newton's second law of motion;
(H1), thermal boundary condition referring to axially constant heat-transfer rate per unit length with constant peripheral wall temperature;
(H2), thermal boundary condition referring to axially constant heat-transfer rate per unit length with constant peripheral wall heat flux;
h, convective heat-transfer coefficient for fully developed laminar flow;
j, Colburn heat-transfer modulus, $StPr^{2/3}$ [dimensionless];
$K(\infty)$, incremental pressure drop number, $\Delta p/(\rho u_m^2/2g_c) - f(4L/D_h)$ [dimensionless];
$K_d(\infty)$, momentum flux correction factor, defined by equation (20);
$K_e(\infty)$, kinetic energy correction factor, defined by equation (21);
k, fluid thermal conductivity;
L_{hy}, hydrodynamic entrance length;
L_{hy}^+, dimensionless hydrodynamic entrance length, $L_{hy}/D_h Re$;
m, number of boundary points;
n, number of unknowns in velocity and temperature problems;
n, s, outer normal and tangential coordinates at a boundary point;
Nu, peripheral average Nusselt number, hD_h/k [dimensionless];
Nu_p, peripheral local Nusselt number [dimensionless];
N_{tu}, number of heat-transfer units, hA/Wc_p [dimensionless];
P, duct perimeter;
$\mathbf{P}$, Householder reflection defined by equation (58), used in Appendix and the section on Golub's method only;
Pr, fluid Prandtl number, $\mu c_p/k$ [dimensionless];
p, porosity [dimensionless];
q'', peripheral average heat flux;
q_p'', peripheral local heat flux;
Re, Reynolds number, $\rho u_m D_h/\mu$ [dimensionless];
r, θ, z, cylindrical polar coordinates;
St, Stanton number, hA_c/Wc_p [dimensionless];
T, temperature defined by equation (31);
t, temperature;
t_c, fluid temperature at the duct centroid;
t_m, fluid bulk mean temperature;
$t_{w,m}$, mean wall temperature defined by equation (44);
$t_{w,\max}^*$, maximum wall temperature $(t_{w,\max} - t_c)/(t_{w,m} - t_c)$ [dimensionless];
$t_{w,\min}^*$, minimum wall temperature $(t_{w,\min} - t_c)/(t_{w,m} - t_c)$ [dimensionless];
u, fluid axial velocity for fully developed laminar flow;
u_m, mean axial velocity, refer equation (19);
$u_{\max}$, maximum axial velocity across the duct cross-section;
W, fluid flow rate;
V, volume of the heat exchanger;
$\mathbf{x}$, an n-vector;
$\mathbf{y}$, an m-vector;
x, y, z, cartesian coordinates;
$\|\mathbf{x}\|^2$, Euclidean norm of a vector $(x_1^2 + \ldots + x_n^2)^{1/2}$;
$\bar{y}$, distance of a centroid of the duct cross-section measured from the base, see Fig. 1;

$\bar{y}_{max}$, normal distance from the base to a point where u_{max} occurs in the duct cross-section;

Greek symbols

α, ratio of heat-transfer area to volume of the exchanger;
α, thermal diffusivity, $k/\rho c_p$;
Δ, RMS error;
Δp, core pressure drop across the heat exchanger;
μ, fluid dynamic viscosity;
ρ, fluid density.

Subscripts

$H1$, (H1) thermal boundary condition;
$H2$, (H2) thermal boundary condition;
i, ith boundary point on duct periphery;
j, jth term of series solution;
m, mean;
T, uniform wall temperature boundary condition;
W, wall.

Superscript

T, transpose of a vector or a matrix.

INTRODUCTION

THE ROLE of a gas turbine engine with a regenerator is becoming increasingly important for vehicular and industrial applications. A highly efficient, low volume, low cost regenerator is a necessity for obtaining superiority over reciprocating and diesel engines.

The first generation of vehicular gas turbine regenerators employed heat-transfer surfaces of triangular flow passage geometry. However, due to manufacturing processes, some of the flow passages of such a regenerator have rounded corners or a sine shape geometry, instead of the idealized uniform triangular shape. The second generation of vehicular gas turbine regenerators may employ rectangular flow passage geometry, because the rectangular flow passage geometry is superior to triangular passage geometry from a heat transfer and flow friction point of view. However, the flow passages, instead of being ideal rectangular, may be trapezoidal or rhombic because of manufacturing limitations. These considerations suggest the need for theoretical solutions for a variety of flow passage geometries.

For a compact regenerator, the flow passages must have a small hydraulic radius. For the low Reynolds number design range of such a regenerator, fully developed laminar flow may prevail along most of the flow length. Thus, fully developed laminar solutions are needed. The determination of such solutions for an arbitrary duct geometry is the subject matter of this paper.

Hydrodynamically and thermally fully developed laminar flow is analyzed for a Newtonian, constant property fluid flowing through a duct of arbitrary but constant cross-section (Fig. 1a). Forced convection heat transfer is considered under a constant axial wall heat-transfer rate per unit length and arbitrary peripheral thermal boundary conditions.

Eight methods have been used in the literature to analyze the aforementioned class of problems for circular and noncircular ducts: (1) the analogy method; (2) the complex variables method; (3) the conformal mapping method; (4) the finite difference method; (5) the point-matching method; (6) the least-squares-matching method; (7) variational methods; and (8) methods for small aspect ratio ducts. These methods are described in some detail by Shah and London [1].

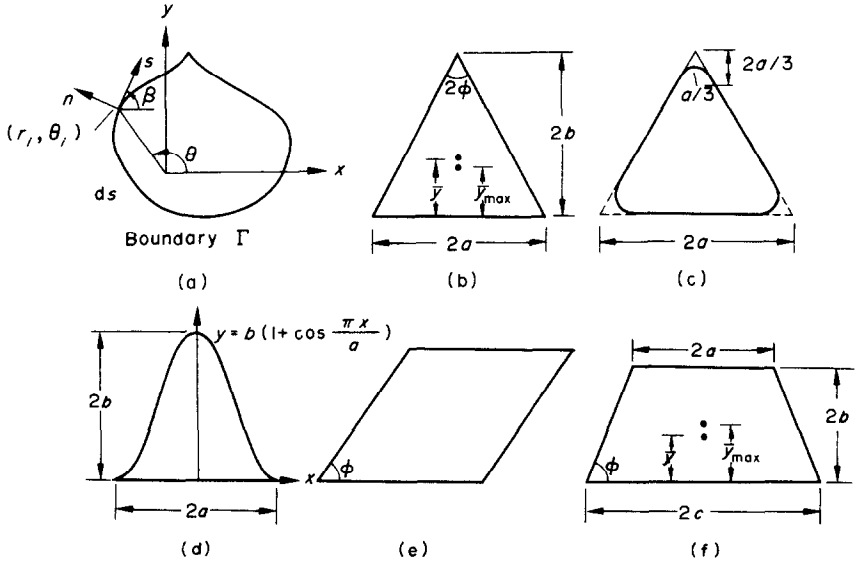

FIG. 1. (a) Duct of arbitrary cross section; (b) isosceles triangular duct; (c) equilateral triangular duct with rounded corners; (d) sine duct; (e) rhombic duct; (f) trapezoidal duct.

Also, some or all of the results fRe, Nu_{H1}, Nu_{H2} and Nu_T obtained by these methods are presented in [1] for twenty-five different duct geometries. The approximate methods (5) and (6) outlined above are powerful, computationally fast and accurate to any desired degree for the axially constant heat flux boundary conditions.

As is demonstrated later, the application of boundary values to fully developed laminar flow velocity and temperature problems reduce to the form of solving the matrix equation (1). In the point-matching method, the number of boundary points chosen for the solution equals the number of unknowns x_j. In contrast, for the least-squares-matching method, a larger number of boundary points are chosen for a better match of the curved or sharp cornered boundaries. Hence, the latter method is preferred for ducts with such boundaries.

Sparrow and Haji-Sheikh [2] proposed such a method of least-squares-matching of boundary values for ducts of arbitrary cross-section. They employed the Gram–Schmidt orthonormalization procedure for the least-squares approximation. However, after experiencing difficulties with the Sparrow and Haji-Sheikh method, an alternative method was devised. This proposed method employs a different, numerically fast and more accurate least-squares approximation due to Golub [3].

After the Golub method is described, the velocity and temperature problems are formulated, followed by the comparison with the Sparrow and Haji-Sheikh method. The application of the method is then made to analyze laminar fluid flow and heat transfer through isosceles triangular, rounded corner equilateral triangular, sine, rhombic and trapezoidal ducts. These geometries are delineated in Fig. 1. Finally the important aspects of the numerical results are discussed from a heat exchanger designer's viewpoint.

THE GOLUB METHOD

The velocity and temperature problems, described below for the laminar flow forced convection heat transfer, reduce to solving of the matrix equation.

$$\mathbf{Ax} = \mathbf{y} \tag{1}$$

where $\mathbf{x} = (x_1, \ldots, x_j, \ldots, x_n)^T$ is a vector whose elements are to be determined. These x_j correspond to the unknown series coefficients a_0, a_j and b_j for the velocity problem, or c_0, c_j and d_j for the temperature problem. The $m \times n$ matrix $\mathbf{A}$ consists of elements which are harmonic polynominals associated with the unknowns x_j. The vector $\mathbf{y} = (y_1, \ldots, y_i, \ldots, y_m)^T$ is known for the m specified boundary points on the duct periphery. As mentioned above, for $m > n$ the exact solution to overdetermined system of equation (1) is not expected. The desired solution is the one which minimizes error ε as defined below, between exact y_i and calculated $y_{i,c}$.

$$\varepsilon = \sum_{i=1}^{m} (y_i - y_{i,c})^2 = \min_{x} \|\mathbf{Ax} - \mathbf{y}\|^2. \tag{2}$$

Choosing $\mathbf{x}$ to minimize ε is called "the method of least-squares". Golub [3] employed Householder reflections to obtain a least-squares solution of equation (1). This method is described below. Golub's method is much less susceptible to trouble from roundoff errors and works for the "ill-conditioned" matrix where the classical method of least-squares based on the "normal equation" approach would fail.

The properties of Householder reflections are described in the Appendix. By successively multiplying equation (1) by Householder reflections $\mathbf{P}_j$, $j = 1, 2, \ldots, n$, the matrix $\mathbf{A}$ is transformed into an upper triangular matrix $\mathbf{U}$ which has at least some nonzero elements only on top of the main diagonal, all elements below main diagonal being zero. Essentially, equation (1) reduces to

$$\mathbf{Ux} = \mathbf{w} \tag{3}$$

where

$$\mathbf{U} = \mathbf{QA}, \quad \mathbf{w} = \mathbf{Qy} \tag{4}$$

and

$$\mathbf{Q} = \mathbf{P}_n \ldots \mathbf{P}_j \ldots \mathbf{P}_2 \mathbf{P}_1. \tag{5}$$

To solve this upper triangular overdetermined system of equation (3), let

$$\tilde{\mathbf{U}} = \text{first } n \text{ rows of } \mathbf{U} \tag{6}$$

and

$$\tilde{\mathbf{w}} = \text{first } n \text{ elements of } \mathbf{w}. \tag{7}$$

Thus $\tilde{\mathbf{U}}$ is an $n \times n$ square upper triangular matrix and $\tilde{\mathbf{w}}$ is an n-vector.

$$\tilde{\mathbf{U}}\mathbf{x} = \tilde{\mathbf{w}} \tag{8}$$

can be solved exactly to determine unknown x_j by the back substitution process of Gaussian elimination method [4]. Employing the orthogonal property of the Householder reflection, it can be shown that the unknowns x_j obtained by solving equation (8) represents a least-squares approximation and the error ε of equation (2) reduces to

$$\varepsilon = w_{n+1}^2 + \ldots + w_m^2. \tag{9}$$

These residues are printed as a part of the computer output in the form Δ_1, Δ_2, etc., as defined later, to establish the accuracy of the least-squares approximation.

VELOCITY PROBLEM

Consider a steady state, fully developed laminar flow in a duct of constant cross-sectional area (Fig. 1a). The fluid is idealized to have ρ, μ, c_p, k all constant. In the absence of body forces, the applicable differential momentum equation is

$$\nabla^2 u = \frac{1}{r}\frac{\partial}{\partial r}\left(r\frac{\partial u}{\partial r}\right) + \frac{1}{r^2}\frac{\partial^2 u}{\partial \theta^2} = \frac{g_c}{\mu}\frac{\mathrm{d}p}{\mathrm{d}z} = c_1. \tag{10}$$

The boundary condition is

$$u = 0 \quad \text{on} \quad \Gamma. \tag{11}$$

By applying the transformation

$$-\frac{u}{c_1} = u^* - \frac{r^2}{4}, \tag{12}$$

equation (10) is reduced to Laplace's equation

$$\nabla^2 u^* = 0 \tag{13}$$

with the boundary condition, equation (11), expressed as

$$u^* = r_i^2/4 \quad \text{on} \quad \Gamma. \tag{14}$$

Here the suffix i denotes the value of a point on the duct boundary Γ. This velocity problem, after the indicated transformation, is a Dirichlet problem and has a unique solution.

The algebraic-trigonometric (harmonic) polynomials,

$$r^j \cos j\theta (j = 0, 1, 2, \ldots), \quad r^j \sin j\theta (j = 1, 2, \ldots) \tag{15}$$

which individually are the solution of Laplace's equation, are chosen for the general solution of equation (13). As the Laplace's equation is linear and homogeneous, the general solution is represented by the sum of such N polynomials.

$$u^* = a_0 + \sum_{j=1}^{N} r^j (a_j \cos j\theta + b_j \sin j\theta) \tag{16}$$

where a_0, a_j and b_j are arbitrary constants to be determined as discussed below.

To apply this solution to the laminar duct flow velocity problem, it must satisfy the boundary condition, equation (14), thus

$$a_0 + \sum_{j=1}^{N} r_i^j (a_j \cos j\theta_i + b_j \sin j\theta_i) = \frac{r_i^2}{4}. \tag{17}$$

Equation (17) represents a_0, a_j and b_j, a total of $n = 2N + 1$ unknown coefficients. The values of r_i and θ_i are provided for m points on the boundary Γ so that m equations are available for n unknowns. The problem essentially reduces to that of solving equation (1) with proper elements of the matrix **A** and the vector **y** from equation (17). These unknown coefficients are determined by Golub's method described earlier. A closed form solution for the velocity distribution is subsequently obtained by combining equations (12) and (16) as

$$-\frac{u}{c_1} = -\frac{r^2}{4} + a_0 + \sum_{j=1}^{N} r^j (a_j \cos j\theta + b_j \sin j\theta). \tag{18}$$

The flow parameters of interest, u_m, $K_d(\infty)$, $K_e(\infty)$, $K(\infty)$, L_{hy}^+ and fRe, are computed from the following definitions or working formulae [1, 2].

$$-\frac{u_m}{c_1} = \frac{1}{A_c} \int_{A_c} \left(-\frac{u}{c_1}\right) dA_c, \tag{19}$$

$$K_d(\infty) = \frac{1}{A_c} \int_{A_c} \left(\frac{u}{u_m}\right)^2 dA_c, \tag{20}$$

$$K_e(\infty) = \frac{1}{A_c} \int_{A_c} \left(\frac{u}{u_m}\right)^3 dA_c, \tag{21}$$

$$K(\infty) = 2[K_e(\infty) - K_d(\infty)], \tag{22}$$

$$fRe = \frac{D_h^2/2}{(-u_m/c_1)}, \tag{23}$$

$$L_{hy}^+ = \frac{(u_{\max}/u_m)^2 - 1 - K(\infty)}{4fRe} \tag{24}$$

where u/u_m, from equations (18) and (23) is given by

$$\frac{u}{u_m} = \frac{2fRe}{D_h^2}\left[-\frac{r^2}{4} + a_0 + \sum_{k=1}^{N} r^j (a_j \cos j\theta + b_j \sin j\theta)\right]. \tag{25}$$

In the numerical evaluation of aforementioned quantities, it is essential to know the accuracy of the approximate solution. As Laplace's equation is being considered, the maximum error (if any) will occur at the boundary points. As these points are matched by a least-squares approximation, the RMS deviation Δ_2 of boundary values

$$\Delta_2 = \left\{\frac{1}{m}\sum_{i=1}^{m}\left[\frac{r_i^2}{4} - a_0 - \sum_{j=1}^{N} r_i^j (a_j \cos j\theta_i + b_j \sin j\theta_i)\right]^2\right\}^{1/2} \tag{26}$$

is computed to determine the degree of precision for the velocity profile. From equations (25) and (26) it can be seen that Δ_1, defined by

$$\Delta_1 = \frac{2fRe}{D_h^2}\Delta_2 \tag{27}$$

compares with u/u_m, the latter being the order of unity.

TEMPERATURE PROBLEM

In addition to idealizations made for the velocity problem, consider no axial heat conduction, viscous dissipation and thermal energy sources within the fluid. Also neglected are the mass diffusion, chemical reaction, and change of phase effects. The applicable differential energy equation for laminar hydrodynamically and thermally developed flow is

$$\nabla^2 t = \frac{u}{\alpha}\frac{\partial t}{\partial z}. \tag{28}$$

The associated thermal boundary condition is considered as axially constant heat-transfer rate per unit duct length, with peripherally arbitrary variation in temperature or heat flux. For this boundary condition and fully developed flow, it can be shown that

$$\frac{\partial t}{\partial z} = \frac{dt_m}{dz} = \frac{q''P}{\rho A_c u_m c_p}. \tag{29}$$

Substituting equations (29) and (25) into (28) yields

$$\nabla^2 T = a_0 - \frac{r^2}{4} + \sum_{j=1}^{N} r^j (a_j \cos j\theta + b_j \sin j\theta) \tag{30}$$

where

$$T = \frac{t}{(8fReq''/kD_h^3)}. \tag{31}$$

Equation (30) is now reduced to Laplace's equation by considering the solution of the form

$$T = T^* + T_p \tag{32}$$

where the particular solution T_p is found as

$$T_p = a_0\frac{r^2}{4} - \frac{r^4}{64} + \sum_{j=1}^{N} \frac{r^{j+2}}{4(j+1)}(a_j \cos j\theta + b_j \sin j\theta), \tag{33}$$

which satisfies equation (30). Substituting equation (32) in (30) yields Laplace's equation

$$\nabla^2 T^* = 0, \tag{34}$$

with the general homogeneous solution as

$$T^* = c_0 + \sum_{j=1}^{N} r^j (c_j \cos j\theta + d_j \sin j\theta). \tag{35}$$

The coefficients c_0, c_j and d_j are determined by the least-squares method from the imposed peripheral boundary conditions such as (i) peripherally prescribed surface temperature, or (ii) peripherally prescribed wall heat flux. The case of an arbitrary combination of peripherally prescribed temperature and wall heat flux can be analyzed in a straightforward manner from the results of the above cases (i) and (ii) [5]. Now attention is directed toward the specific solutions for the foregoing two peripheral boundary conditions.

Peripherally prescribed surface temperature

The surface temperature of the duct periphery is prescribed as $t(r_i, \theta_i)$. Applying equation (32) at the boundary points, one gets

$$c_0 + \sum_{j=1}^{N} r_i^j (c_j \cos j\theta_i + d_j \sin j\theta_i) = T^* = T(r_i, \theta_i) - T_p(r_i, \theta_i) \tag{36}$$

where c_0, c_j and d_j are $n = 2N+1$ unknowns. For m prescribed boundary points and for $m > n$, equation (36) represents a linear least-squares problem, identical to the velocity problem, and is solved using Golub's method. Once the unknown coefficients are determined, the closed-form solution for the temperature distribution is found by substituting equations (33) and (35) into equation (32). The other parameters of interest, t_m, q_p'' and Nu_p and Nu are computed as follows:

$$\frac{t_m}{\dfrac{q''}{k} \cdot \dfrac{8fRe}{D_h^3}} = \frac{1}{A_c} \int_{A_c} \left(\frac{u}{u_m}\right) T \, \mathrm{d}A_c, \tag{37}$$

$$q_p'' = k \frac{\partial t}{\partial n} = k \left(\frac{\partial t}{\partial r} \frac{\partial r}{\partial n} + \frac{\partial t}{\partial \theta} \frac{\partial \theta}{\partial n} \right), \tag{38}$$

where from Fig. 1(a)

$$\frac{\partial r}{\partial n} = \sin(\theta - \beta), \quad \frac{\partial \theta}{\partial n} = \frac{1}{r} \cos(\theta - \beta) \tag{39}$$

and from equations (32) and (31),

$$\frac{\partial t}{\partial r} = \frac{q''}{k} \frac{8fRe}{D_h^3} \left[\sum_{j=1}^{N} j r^{j-1} (c_j \cos j\theta + d_j \sin j\theta) + \left(a_0 \frac{r}{2} - \frac{r^3}{16} \right) + \sum_{j=1}^{N} \frac{(j+2) r^{j+1}}{4(j+1)} \times (a_j \cos j\theta + b_j \sin j\theta) \right], \tag{40}$$

$$\frac{\partial t}{\partial \theta} = \frac{q''}{k} \frac{8fRe}{D_h^3} \left[\sum_{j=1}^{N} j r^j (d_j \cos j\theta - c_j \sin j\theta) + \sum_{j=1}^{N} \frac{j r^{j+2}}{4(j+1)} (b_j \cos j\theta - a_j \sin j\theta) \right]. \tag{41}$$

The peripheral local and average Nusselt numbers are evaluated from

$$Nu_P = \frac{q_p'' D_h}{k} \frac{1}{t_w - t_m}, \tag{42}$$

$$Nu = \frac{h D_h}{k} = \frac{(q'/P) D_h}{k} \frac{1}{t_{w,m} - t_m}, \tag{43}$$

where

$$t_{w,m} = \frac{1}{P} \int_{\Gamma} t(r_i, \theta_i) \, \mathrm{d}s. \tag{44}$$

A special case of above generalized peripheral temperature variation is the peripherally constant wall temperature, $t(r_i, \theta_i) = t_w$ = a constant, corresponding to the (H1) boundary condition. The foregoing analysis remains the same; except for convenience, T in equation (31) is redefined using $(t - t_w)$ in place of t. Correspondingly, $T(r_i, \theta_i) = 0$ in equation (36), the l.h.s. of equation (37) represents $(t_m - t_w)$ instead of t_m and the Nusselt number expression of equation (43) becomes

$$Nu_{H1} = -\frac{D_h^4}{8fRe} \left[\frac{1}{A_c} \int_{A_c} \left(\frac{u}{u_m} \right) T \, \mathrm{d}A_c \right]^{-1}. \tag{45}$$

The boundary RMS error, designated as Δ_3, for the (H1) temperature problem is calculated from

$$\Delta_3 = \left\{ \frac{1}{m} \sum_{i=1}^{m} \left[-T_p(r_i, \theta_i) - c_0 - \sum_{j=1}^{N} r_i^j (c_j \cos j\theta_i + d_j \sin j\theta_i) \right]^2 \right\}^{1/2}. \tag{46}$$

Peripherally prescribed wall heat flux

For this problem, the heat flux around the duct periphery Γ is specified as $q''(r_i, \theta_i) = q_p''$. This heat flux is related to the fluid temperature gradient at the wall by equation (38). Substituting the values of $\partial t/\partial r$ and $\partial t/\partial \theta$ from equations (40) and (41) in equations (38) and after rearrangement, one finds that

$$\sum_{j=1}^{N} \left[c_j \{ j r_i^{j-1} (l' \cos j\theta_i - m' r_i \sin j\theta_i) \} + d_j \{ j r_i^{j-1} (l' \sin j\theta_i + m' r_i \cos j\theta_i) \} \right] = \frac{q_p''}{q'' \dfrac{8fRe}{D_h^3}} - l' \left(a_0 \frac{r_i}{2} - \frac{r_i^3}{16} \right) - \sum_{j=1}^{N} \frac{r_i^{j+1}}{4(j+1)} \times \left[a_j \{ l'(j+2) \cos j\theta_i - m' j r_i \sin j\theta_i \} + b_j \{ l'(j+2) \sin j\theta_i + m' j r_i \cos j\theta_i \} \right], \tag{47}$$

where

$$l' = \left. \frac{\partial r}{\partial n} \right|_{(r_i, \theta_i)} = \sin(\theta_i - \beta_i), \tag{48}$$

$$m' = \left. \frac{\partial \theta}{\partial n} \right|_{(r_i, \theta_i)} = \frac{1}{r_i} \cos(\theta_i - \beta_i). \tag{49}$$

Equation (47) represents c_j and d_j as unknown coefficients, a total of $2N$, and are evaluated by the least-squares method. Subsequently, the closed form temperature distribution is obtained from equation (32) at the boundary points (r_i, θ_i). The fluid bulk mean temperature and peripheral local and average Nusselt numbers can readily be computed from their definitions.

Note that the coefficient c_0 in equation (35) for this Neumann problem cannot be determined. The solution to this problem is unique only within an arbitrary constant. This constant can only be determined from an additional physical constraint such as the specification of magnitude of temperature at one point on the wall or in the flow field. However, for the determination of Nu, the value of c_0 is not needed, as it cancels from the equation.

Consider the special case of $q_p'' = q'' =$ a constant. This corresponds to the (H2) boundary condition. For this case, t_m is evaluated from equation (37) and $t_{w,m}$ from equation (44), and Nu_{H2} from the following equation which is based on equation (43).

$$Nu_{H2} = \frac{D_h^4/8fRe}{\frac{1}{P}\int_\Gamma T(r_i,\theta_i)\,\mathrm{d}s - \frac{1}{A_c}\int_{A_c}\left(\frac{u}{u_m}\right)T\,\mathrm{d}A_c}. \quad (50)$$

The boundary RMS error Δ_4 for the (H2) temperature problem is determined from

$$\Delta_4 = \left\{\frac{1}{m}\sum_{i=1}^{m}(q_i - q_{i,\mathrm{cal}})^2\right\}^{1/2}, \quad (51)$$

where q_i represents the r.h.s. of equation (47) and $q_{i,\mathrm{cal}}$ denotes the l.h.s. of equation (47) with c_j and d_j calculated by the least-squares technique.

COMPARISON WITH SPARROW AND HAJI-SHEIKH'S METHOD

As mentioned earlier, the least-squares-matching methods are powerful and highly accurate results can be obtained for fully developed laminar forced convection in a constant cross-section duct. Sparrow and Haji-Sheikh [2] were the first investigators to apply such a method to the above problem. They employed the well-known Gram–Schmidt orthonormalization technique for the least-squares approximation. However, other numerically fast and more accurate least-squares approximation methods exist in the literature. One such method due to Golub is employed in the present paper. The following comparison presents where exactly the improvement over the Sparrow and Haji-Sheikh (SH) method is obtained.

The SH method employs the Gram–Schmidt orthonormalization technique to generate othonormal functions Φ_j. These Φ_j are calculated as an intermediate step and are not needed once the unknown coefficients x_j are determined. Hence, the SH method utilizes more computer time and storage and has more roundoff errors than the present more direct method. Additionally, in the SH method, equidistant points on the boundary Γ are required for a contour integration around the boundary for the determination of Φ_j. In the present method, equidistant points are not a requirement.

The SH method employs real and imaginary parts of the complex variable $Z^N = (x+iy)^N$, in cartesian coordinate system with $N = 0$ to 8, for the general solution of the Laplace equation. To obtain 1 per cent or better accuracy in final results, the first seventeen functions ($n = 2N+1 = 17$) are insufficient for the ducts presently considered. Even though the higher harmonic functions ($N > 8$) can be determined by a complex algorithm, it is a cumbersome task to determine the other required functions for the SH method for higher values of N. The present method employs real and imaginary parts of a complex variable Z^N in a cylindrical coordinate system with N varying from 0 to 40; but with no difficulties for even higher order functions ($N > 40$). Additionally, in the SH method, each harmonic function contains positive and negative terms of x and y having large powers for large N. Computationally, this increases roundoff errors. In the present method, roundoff errors are minimized because (1) the use of the cylindrical coordinate system and (2) the trick of adjusting the size of each duct geometry to $D_h = 2$.

The accuracy obtained in the results by the present method is discussed in the following section, where also is indicated that a further refinement in the least-squares solution may be obtained by the Chebyshev method [12].

NUMERICAL RESULTS FOR TRIANGULAR, SINE, RHOMBIC AND TRAPEZOIDAL DUCTS

As a technically interesting application of the foregoing method, the triangular, sine, rhombic and trapezoidal ducts of Fig. 1 were investigated. A double precision program was written in Fortran IV-H language for IBM 360/67 and 370/145 computers. All the details of numerical computations and the computer program are presented in [5]. Some salient points are summarized below.

Area integrations of equations (19), (20), (21) and (37) were evaluated using the Newton–Cotes 7-point closed type composite integration formula [4]. The contour integration, to evaluate $t_{w,m}$, was performed using the trapezoidal composite integration formula; because this method is believed to be more accurate for a closed contour than the higher order Newton–Cotes formulae. A total of 83 to 91 points were taken along the boundary of the ducts considered. N in the series solutions was specified from 30 to 40 with 40 used for the most ducts.

Important geometrical properties and numerical results obtained for flow and heat transfer are summarized in Tables 1–5. Some of these results are also presented in Figs. 2–5. For completeness, results for the limiting duct geometries of $2b/2a = \infty$ and 0 from [1] are included. Note that when $2a = 0$ (see Fig. 1), the trapezoidal duct reduces to an isosceles triangular duct. Also included is Nu_T for the isosceles triangular and sine ducts from [6] and [7] respectively.

Table 1. Isosceles triangular ducts geometrical, flow and heat-transfer characteristics for fully developed laminar flow*

$\frac{2b}{2a}$	2ϕ	$\frac{\bar{y}}{2a}$	$\frac{\bar{y}_{max}}{2a}$	$\frac{u_{max}}{u_m}$	$K_d(\infty)$	$K_e(\infty)$	$K(\infty)$	L_{hy}^+	fRe	Nu_T	Nu_{H1}	Nu_{H2}	$t^*_{w,max}$	$t^*_{w,min}$
∞	0	–	–	3·000	1·600	3·086	2·971	·1048	12·000	0·943	2·059	0	–	–
8·000	7·15	2·66667	·83592	2·593	1·545	2·805	2·521	·0648	12·352	1·46	2·348	0·039	–	–
5·715	10·00	1·90501	·74009	2·521	1·526	2·731	2·409	·0590	12·474	1·61	2·446	0·080	–	–
4·000	14·25	1·33333	·64240	2·442	1·505	2·640	2·271	·0533	12·636	1·81	2·575	0·173	4·14	–
2·836	20·00	0·94521	·55282	2·368	1·482	2·546	2·128	·0484	12·822	2·00	2·722	0·366	4·07	–
2·000	28·07	0·66667	·46729	2·302	1·459	2·454	1·991	·0443	13·026	2·22	2·880	0·747	3·83	·073
1·866	30·00	0·62201	·45102	2·290	1·455	2·438	1·966	·0436	13·065	2·26	2·910	0·851	3·73	·127
1·500	36·87	0·50000	·40140	2·259	1·443	2·392	1·898	·0418	13·181	2·36	2·998	1·22	3·38	·287
1·374	40·00	0·45791	·38215	2·249	1·439	2·377	1·876	·0412	13·222	2·39	3·029	1·38	3·17	·347
1·072	50·00	0·35742	·33033	2·228	1·431	2·347	1·831	·0401	13·307	2·45	3·092	1·76	2·53	·469
1·000	53·13	0·33333	·31641	2·225	1·430	2·342	1·824	·0399	13·321	2·46	3·102	1·82	2·41	·483
0·866	60·00	0·28868	·28868	2·222	1·429	2·338	1·818	·0398	13·333	2·47	3·111	1·892	1·79	·515
0·750	67·38	0·25000	·26231	2·225	1·430	2·342	1·824	·0399	13·321	2·45	3·102	1·84	1·99	·499
0·714	70·00	0·23803	·25364	2·227	1·431	2·345	1·829	·0400	13·311	2·45	3·095	1·80	2·04	·488
0·596	80·00	0·19863	·22313	2·241	1·436	2·366	1·860	·0408	13·248	2·40	3·050	1·59	2·19	·432
0·500	90·00	0·16667	·19584	2·264	1·445	2·400	1·909	·0421	13·153	2·34	2·982	1·34	2·30	·364
0·289	120·00	0·09623	·12552	2·380	1·489	2·571	2·165	·0490	12·744	2·00	2·680	0·62	2·45	·167
0·250	126·87	0·08333	·11085	2·416	1·499	2·617	2·235	·0515	12·622	1·90	2·603	0·490	2·47	·131
0·134	150·00	0·04466	·06301	2·587	1·543	2·815	2·543	·0644	12·226	1·50	2·325	0·156	2·56	·045
0·125	151·93	0·04167	·05907	2·605	1·548	2·835	2·574	·0659	12·196	1·47	2·302	0·136	2·65	·038
0	180·00	0·00000	·00000	3·000	1·600	3·086	2·971	·1048	12·000	0·943	2·059	0	–	–

*$P/2a = 1+\sqrt{[1+(2b/a)^2]}$, $A_c/(2a)^2 = b/2a$.

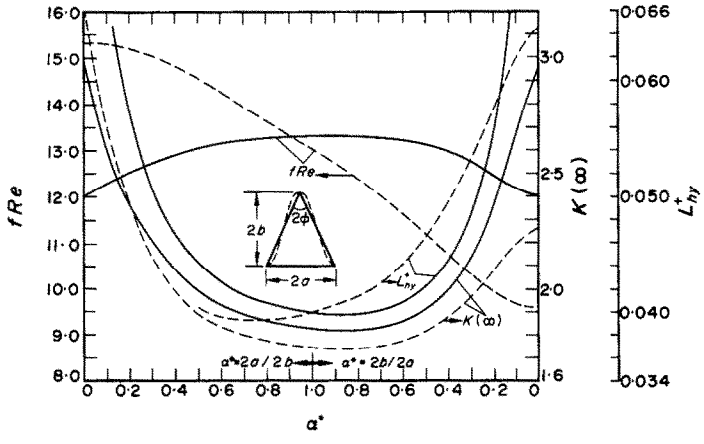

FIG. 2. Isosceles triangular and sine ducts $K(\infty)$, L_{hy}^+ and fRe for fully developed laminar flow.

Table 2. Rounded corner equilateral triangular ducts geometrical, flow and heat-transfer characteristics for fully developed laminar flow

	0 rounded corner	1 rounded corner	2 rounded corner	3 rounded corner
$P/2a$	3·00000	2·77172	2·54343	2·31515
$A_c/(2a)^2$	0·43301	0·41399	0·39497	0·37594
$D_h/2a$	0·57735	0·59745	0·62115	0·64953
$\bar{y}/2a$	0·28868	0·26778	0·30957	0·28868
$\bar{y}_{max}/2a$	0·28868	0·28627	0·29117	0·28868
u_{max}/u_m	2·222	2·172	2·115	2·064
$K_d(\infty)$	1·429	1·406	1·379	1·353
$K_e(\infty)$	2·338	2·254	2·163	2·074
$K(\infty)$	1·818	1·698	1·567	1·441
L_{hy}^+	0·0398	0·0359	0·0319	0·0284
fRe	13·333	14·057	14·899	15·993
Nu_{H1}	3·111	3·401	3·756	4·205
Nu_{H2}	1·892	2·196	2·715	3·780
$t^*_{w,max}$	1·79	2·03	2·42	1·22
$t^*_{w,min}$	0·515	0·512	0·550	0·757

The coefficients in equations (17), (35) and (47) for the velocity and temperature problems and the RMS errors Δ_1 to Δ_4 are reported in [5].*

Except for the rhombic ducts, the maximum velocity does not occur at the centroid of the cross-section, but rather occurs on the axis of symmetry away from the centroid. The distance $\bar{y}$ of the centroid and $\bar{y}_{max}$ (where the maximum velocity occurs), both measured from the base, are also reported in these tables.

The wall temperature around the duct periphery is

*The coefficients b_j of equation (18) and d_j of equation (35) are zero for a duct symmetrical about one axis and when θ is measured from the axis of symmetry. The coefficients a_j for the velocity problem and c_j for the (H1) and (H2) temperature problems are determined for the rectangular, isosceles triangular, rounded corner triangular, sine, rhombic and trapezoidal ducts. They are deposited as Document No. NAPS 02464 with the National Auxiliary Publications Service, c/o Microfiche Publications, 440 Park Avenue South, New York, NY 10016.

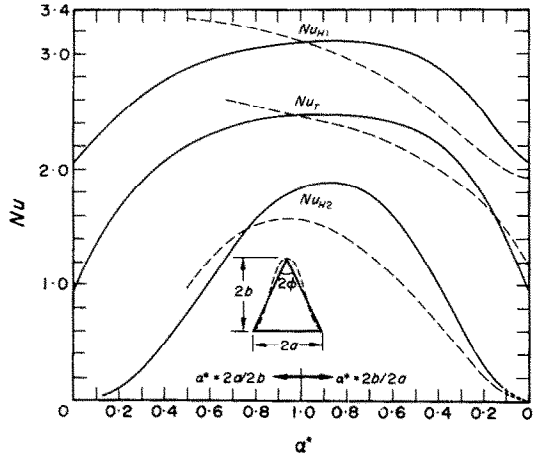

FIG. 3. Isosceles triangular and sine ducts Nu_{H1}, Nu_{H2} and Nu_T for fully developed laminar flow.

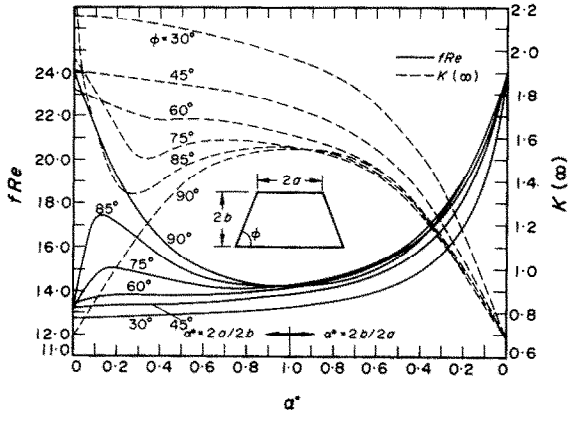

FIG. 4. Trapezoidal ducts fRe and $K(\infty)$ for fully developed laminar flow.

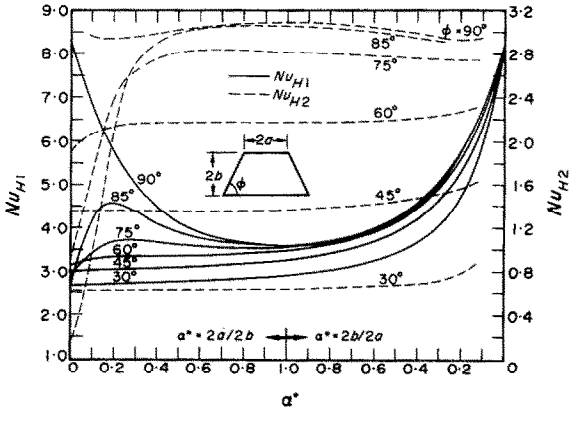

FIG. 5. Trapezoidal ducts Nu_{H1} and Nu_{H2} for fully developed laminar flow.

Table 3. Sine ducts geometrical, flow and heat-transfer characteristics for fully developed laminar flow*

$\frac{2b}{2a}$	$\frac{P}{2a}$	$\frac{D_h}{2a}$	$\frac{\bar{y}}{2a}$	$\frac{\bar{y}_{max}}{2a}$	$\frac{u_{max}}{u_m}$	$K_d(\infty)$	$K_e(\infty)$	$K(\infty)$	L^+_{hy}	fRe	Nu_T	Nu_{H1}	Nu_{H2}	$t^*_{w,max}$	$t^*_{w,min}$
∞	–	–	–	–	3·825	1·604	3·213	3·218	·1701	15·303	0·739	2·521	0	–	–
2	5·1898	·77074	0·75000	·46494	2·2848	1·435	2·376	1·884	·0403	14·553	–	3·311	0·95	2·92	·002
3/2	4·1315	·70897	0·56250	·40964	2·2239	1·423	2·326	1·806	·0394	14·022	2·60	3·267	1·38	2·93	·257
$1/\sqrt{3}/2$	3·3049	·60516	0·37500	·33390	2·2197	1·414	2·286	1·744	·0400	13·023	2·45	3·102	1·55	2·17	·398
	3·0667	·56479	0·32476	·30773	2·2191	1·414	2·283	1·739	·0408	12·630	–	3·014	1·47	2·58	·396
3/4	2·8663	·52332	0·28125	·28205	2·2190	1·415	2·287	1·744	·0419	12·234	2·33	2·916	1·34	2·93	·379
1/2	2·4637	·40589	0·18750	·21347	2·2211	1·429	2·334	1·810	·0464	11·207	2·12	2·617	0·90	3·65	·266
1/4	2·1398	·23366	0·09375	·11926	2·2291	1·467	2·474	2·013	·0553	10·123	1·80	2·213	0·33	4·16	·099
1/8	2·0375	·12270	0·04688	·06173	2·2357	1·496	2·582	2·173	·0612	9·743	–	2·017	0·095	4·31	·030
0	2·0000	·00000	0·00000	·00000	2·2400	1·512	2·646	2·271	·0648	9·600	1·178	1·920	0	–	–

* $A_c/(2a)^2 = b/2a$.

nonuniform for the (H2) boundary condition. A hot spot occurs at one of the corners of the noncircular duct and a cold spot occurs on one of the sides. The corresponding dimensionless maximum and minimum wall temperatures, $t^*_{w,max}$ and $t^*_{w,min}$, are presented in Tables 1–6.

In order to assess the accuracy of the present method, calculations were also made for rectangular ducts with aspect ratio varying from 1 to $\frac{1}{8}$. Some of these results are presented in Table 6 [1,5]. The u_{max}/u_m, $K_d(\infty)$, $K_e(\infty)$, $K(\infty)$, L^+_{hy}, fRe and Nu_{H1} results presently determined for all the rectangular and the equilateral

Table 4. Rhombic ducts flow and heat-transfer characteristics for fully developed laminar flow

ϕ	$\frac{u_{max}}{u_m}$	$K_d(\infty)$	$K_e(\infty)$	$K(\infty)$	L^+_{hy}	fRe	Nu_{H1}	Nu_{H2}	$t^*_{w,max}$	$t^*_{w,min}$
90	2.096	1.378	2.154	1.551	0.0324	14.227	3.608	3.09	1.39	0.769
80	2.102	1.381	2.163	1.564	0.0327	14.181	3.581	2.97	1.65	0.743
70	2.120	1.389	2.190	1.603	0.0336	14.046	3.500	2.64	1.86	0.671
60	2.151	1.402	2.239	1.673	0.0353	13.830	3.367	2.16	2.05	0.565
50	2.199	1.422	2.311	1.778	0.0380	13.542	3.188	1.62	2.21	0.439
45	2.230	1.436	2.361	1.850	0.0397	13.381	3.080	1.34	2.27	0.372
40	2.266	1.448	2.411	1.925	0.0419	13.193	2.969	1.09	2.32	0.307
30	2.359	1.481	2.541	2.120	0.0477	12.803	2.722	0.624	2.40	0.185
20	2.493	1.521	2.713	2.384	0.0570	12.416	2.457	0.279	2.45	0.089
10	2.689	1.562	2.908	2.693	0.0732	12.073	2.216	0.070	2.46	0.023
0	3.000	1.600	3.086	2.971	0.1048	12.000	2.059	0	–	–

Table 5. Trapezoidal ducts geometrical, flow and heat-transfer characteristics for fully developed laminar flow

$\frac{2b}{2a}$	$\frac{\bar{y}}{2a}$	$\frac{\bar{y}_{max}}{2a}$	$\frac{u_{max}}{u_m}$	$K_d(\infty)$	$K_e(\infty)$	$K(\infty)$	L^+_{hy}	fRe	Nu_{H1}	Nu_{H2}	$t^*_{w,max}$	$t^*_{w,min}$
					$\phi = 85°$							
∞	1.90501	.74009	2.521	1.526	2.731	2.409	.0590	12.474	2.446	0.08	–	–
8	1.43804	.74010	2.186	1.368	2.147	1.557	.0318	17.474	4.366	1.22	–	–
4	1.07487	.73895	2.025	1.336	2.008	1.343	.0262	16.740	4.483	2.54	2.24	.297
2	.70399	.66375	2.045	1.362	2.092	1.461	.0287	15.015	3.896	3.01	1.55	.554
4/3	.52173	.52482	2.091	1.377	2.149	1.543	.0320	14.312	3.636	3.05	1.52	.687
1	.41413	.42131	2.096	1.379	2.155	1.552	.0324	14.235	3.608	3.05	1.55	.716
3/4	.32469	.33057	2.070	1.371	2.125	1.508	.0305	14.576	3.736	3.04	1.56	.611
1/2	.22668	.22982	1.981	1.345	2.028	1.367	.0248	15.676	4.175	2.98	1.64	.478
1/4	.11891	.11976	1.768	1.286	1.821	1.069	.0144	18.297	5.363	2.91	1.87	.305
1/8	.06094	.06116	1.627	1.245	1.683	0.875	.00936	20.599	6.501	2.89	2.18	.190
0	–	–	1.500	1.200	1.543	0.686	.00588	24.000	8.235	–	–	–
					$\phi = 75°$							
∞	.62201	.45102	2.290	1.455	2.438	1.966	.0436	13.065	2.910	0.851	3.73	.127
8	.58459	.45100	2.219	1.415	2.300	1.770	.0362	14.907	3.520	1.90	2.43	.369
4	.52650	.44990	2.141	1.385	2.185	1.560	.0331	14.959	3.720	2.57	1.61	.511
2	.42654	.42537	2.107	1.382	2.166	1.569	.0327	14.340	3.610	2.82	1.73	.611
4/3	.35472	.37226	2.112	1.385	2.177	1.584	.0332	14.118	3.542	2.83	1.76	.704
1	.30261	.32029	2.099	1.381	2.163	1.563	.0323	14.252	3.594	2.82	1.78	.612
3/4	.25257	.26619	2.063	1.370	2.121	1.502	.0298	14.697	3.766	2.81	1.79	.533
1/2	.18940	.19707	1.968	1.343	2.020	1.354	.0240	15.804	4.219	2.78	1.85	.432
1/4	.10793	.11023	1.763	1.286	1.819	1.066	.0142	18.313	5.371	2.75	2.03	.286
1/8	.05794	.05858	1.627	1.246	1.684	0.877	.00936	20.556	6.482	2.76	2.30	.181
0	–	–	1.500	1.200	1.543	0.686	.00588	24.000	8.235	–	–	–
					$\phi = 60°$							
∞	.28868	.28868	2.222	1.429	2.338	1.818	.0398	13.333	3.111	1.89	1.79	.515
8	.28366	.28861	2.205	1.419	2.303	1.770	.0377	13.867	3.284	2.09	1.96	.520
4	.27315	.28749	2.181	1.409	2.267	1.716	.0367	13.916	3.348	2.16	2.03	.514
2	.24819	.27568	2.162	1.404	2.248	1.687	.0360	13.804	3.350	2.17	2.07	.540
4/3	.22445	.25304	2.146	1.400	2.232	1.664	.0350	13.888	3.390	2.17	2.07	.490
1	.20374	.22860	2.119	1.392	2.201	1.618	.0331	14.151	3.495	2.17	2.07	.442
3/4	.18072	.20001	2.071	1.378	2.148	1.539	.0299	14.637	3.691	2.18	2.09	.401
1/2	.14666	.15841	1.969	1.349	2.039	1.379	.0239	15.693	4.140	2.20	2.13	.342
1/4	.09292	.09700	1.766	1.291	1.833	1.084	.0143	18.053	5.247	2.26	2.26	.242
1/8	.05339	.05462	1.634	1.251	1.700	0.897	.00950	20.304	6.341	2.31	2.47	.158
0	–	–	1.500	1.200	1.543	0.686	.00588	24.000	8.235	–	–	–
					$\phi = 45°$							
∞	.16667	.19584	2.264	1.445	2.400	1.909	.0421	13.153	2.982	1.35	2.29	.364
8	.16558	.19575	2.258	1.442	2.388	1.893	.0414	13.301	3.030	1.35	2.29	.364
4	.16296	.19480	2.250	1.439	2.377	1.876	.0410	13.323	3.048	1.35	2.30	.344
2	.15556	.18829	2.232	1.434	2.358	1.847	.0400	13.364	3.081	1.35	2.30	.326
4/3	.14719	.17716	2.206	1.427	2.328	1.803	.0381	13.541	3.155	1.36	2.30	.294
1	.13889	.16483	2.169	1.418	2.290	1.744	.0355	13.827	3.268	1.37	2.31	.277
3/4	.12857	.14945	2.109	1.398	2.218	1.639	.0317	14.260	3.469	1.40	2.32	.263
1/2	.11111	.12495	1.998	1.367	2.099	1.464	.0251	15.206	3.888	1.44	2.35	.236
1/4	.07778	.08333	1.787	1.303	1.875	1.142	.0151	17.397	4.943	1.55	2.46	.180
1/8	.04815	.05000	1.652	1.266	1.737	0.943	.00996	19.743	6.034	1.61	2.65	.122
0	–	–	1.500	1.200	1.543	0.686	.00588	24.000	8.235	–	–	–
					$\phi = 30°$							
∞	.09623	.12552	2.380	1.489	2.571	2.165	.0490	12.744	2.680	.621	2.45	.167
8	.09600	.12543	2.375	1.484	2.558	2.146	.0489	12.760	2.697	.625	2.45	.164
4	.09541	.12482	2.371	1.484	2.555	2.141	.0485	12.782	2.704	.624	2.44	.163
2	.09351	.12170	2.352	1.482	2.540	2.115	.0469	12.875	2.736	.622	2.44	.146
4/3	.09105	.11676	2.310	1.468	2.486	2.038	.0442	13.012	2.821	.635	2.44	.141
1	.08834	.11121	2.266	1.457	2.442	1.969	.0408	13.246	2.919	.640	2.46	.137
3/4	.08459	.10397	2.200	1.441	2.373	1.864	.0363	13.599	3.077	.652	2.47	.133
1/2	.07735	.09148	2.073	1.404	2.229	1.651	.0287	14.323	3.436	.685	2.55	.126
1/4	.06024	.06699	1.850	1.344	1.988	1.288	.0174	16.284	4.349	.744	2.83	.103
1/8	.04103	.04361	1.678	1.272	1.768	0.992	.0112	18.479	5.569	.888	2.89	.080
0	–	–	1.500	1.200	1.543	0.686	.00588	24.000	8.235	–	–	–

Table 6. Rectangular ducts [$\phi = 90°$ in Fig. 1(f)] flow and heat-transfer characteristics for fully developed laminar flow

$\frac{2b}{2a}$	$\frac{u_{max}}{u_m}$	$K_d(\infty)$	$K_e(\infty)$	$K(\infty)$	L^+_{hy}	fRe	Nu_T	Nu_{H1}	Nu_{H2}	$t^*_{w,max}$	$t^*_{w,min}$
1.000	2.096	1.378	2.154	1.552	.0324	14.227	2.976	3.608	3.091	1.39	.769
0.750	2.077	1.373	2.133	1.520	.0310	14.476	–	3.701	3.07	1.41	.649
0.500	1.992	1.347	2.039	1.383	.0255	15.548	3.391	4.123	3.02	1.50	.499
0.250	1.774	1.288	1.826	1.076	.0147	18.233	4.439	5.331	2.94	1.76	.311
0.125	1.628	1.245	1.685	0.879	.00938	20.585	5.597	6.490	2.94	2.11	.192
0	1.500	1.200	1.543	0.686	.00588	24.000	7.541	8.235	–	–	–

triangular ducts differ by less than 0·01 per cent when compared to the best literature values [1]. Corresponding values for isosceles triangular ducts, Table 1, are in excellent agreement with Sparrow and Haji-Sheikh's results [8]. The Table 3 results for sine ducts are in good agreement with the limited results obtained by Sherony and Solbrig [7] using a finite difference method. Nu_{H1} for the rhombic ducts are within 0·1 per cent of those by Iqbal *et al.* [9]. From these comparisons and knowing the values of Δ_1, Δ_2 and Δ_3 are less than 10^{-5} for most of the ducts, it is concluded that the present method will provide numerical results accurate to within 0·05 per cent for those ducts with straight boundaries or those not having very narrow corner regions and within 1 per cent for those ducts with sharp curved boundaries or those having very narrow corners.

The only literature values available for Nu_{H2} are for square and equilateral triangular ducts [10], rectangular ducts, and rhombic ducts with $90° \leqslant \phi \leqslant 60°$ [11]. Values obtained using the proposed method are within 0·3 per cent of these literature values. The accuracy for Nu_{H2} is not as good as for Nu_{H1} because of the "differentiation process" involved in the boundary values of the fluid temperature, equation (38). The accuracy can be improved, if desired, by some of the suggestions in [5]. From the foregoing comparisons, and knowing $10^{-3} \leqslant \Delta_4 \leqslant 10^{-7}$, it is concluded that the Nu_{H2} results are accurate with 1 per cent for those ducts with straight boundaries or those not having very narrow corners and within 5 per cent for those ducts with sharp curved boundaries or those having very narrow corners.

A further refinement in the least-squares solution may be obtained by employing the Chebyshev method [12] instead of the Golub method. The Chebyshev method checks the error of all boundary points individually and minimizes the maximum error of any boundary point. The Golub method minimizes the sum of squares of errors of all boundary points.

DISCUSSION ON INFLUENCE OF PASSAGE GEOMETRIES

Two preliminary questions involved in a new heat exchanger design are (1) how to compare the performance of different idealized passage geometries and (2) if the actual passage geometry differs markedly from the idealized passage geometry due to manufacturing process, how to assess these effects on heat transfer and pressure drop.

Comparison of different idealized passage geometries

The performance of heat exchanger cores made up of different idealized passage geometries may be compared in the following two complimentary ways: (1) comparing the flow area "goodness" factors j/f; and (2) comparing the core volume "goodness" factors h_{std} vs E_{std}.

It can be shown that the flow area goodness factor j/f can be expressed as

$$\frac{j}{f} = \frac{NuPr^{-1/3}}{fRe} = \frac{1}{A_c^2}\left(\frac{Pr^{2/3}}{2g_c\rho}\frac{N_{tu}W^2}{\Delta p}\right). \tag{52}$$

From the first equality in the above equation, j/f is constant for fully developed laminar flow of a specified fluid. From the second equality, this area goodness factor derives its name as it is inversely proportional to A_c^2 (A_c = core free flow area) for the bracketed quantities being constant. The dimensionless j and f factors characterize the shape of geometry and are independent of the scale of the geometry (D_h). Hence, the area goodness factor j/f for different surfaces, when compared, represents the influence of the differences in nondimensional geometric factors. j_{H1}/f is presented in Fig. 6 for the rectangular, trapezoidal,

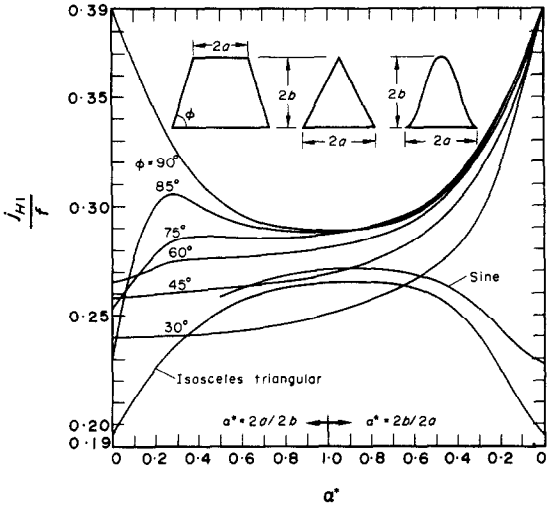

FIG. 6. Isosceles triangular, sine and trapezoidal ducts j_{H1}/f for fully developed laminar flow.

sine and isosceles triangular ducts. This factor ranges from 0·265 (equilateral triangular duct) to 0·390 (parallel plates). Thus the parallel plates geometry, relative to the equilateral triangular duct, presents an improvement of 47 per cent (= 0·390/0·265 − 1) for j_{H1}/f and consequently requires an 18 per cent ($1 - 1/\sqrt{1{\cdot}47}$) smaller free flow area. Very sharp cornered isosceles triangular ducts ($\alpha^* \simeq 0$) have the poorest flow area goodness factor ($j_{H1}/f = 0{\cdot}195$).

The exchanger porosity must be considered in order to translate this free flow area advantage into a frontal area improvement. Note that in the flow area "goodness" factor comparison, no estimate of total heat-transfer area or the volume can be inferred. This is the function of the volume "goodness" factor to be described below.

The core volume "goodness" factor is characterized by a high position for the plot of h_{std} vs E_{std}, where

$$h_{std} = \frac{k}{D_h}Nu = \frac{c_p\mu}{Pr^{2/3}}\frac{1}{D_h}jRe, \tag{53}$$

$$E_{std} = \frac{W\Delta p}{\rho A} = \frac{\mu^3}{2g_c\rho^2}\frac{1}{D_h^3}fRe^3. \tag{54}$$

From the first equality in equation (53), h_{std} is constant for fully developed laminar flow through a constant cross-sectional duct. The expression for E_{std} in equation (54) rigorously applies to a constant density fully developed laminar flow. For such a flow, Δp is proportional to W, hence E_{std} is proportional to W^2. Unlike the j/f factors, h_{std} and E_{std} are dependent upon the scale of the surface geometry as found from equations (53) and (54). Hence, for comparison of different surface geometries, a common hydraulic diameter $D_h = 0{\cdot}002$ ft (0·61 mm) is used to eliminate the influence of geometrical scale. Also the physical properties* employed in equations (53) and (54) are for dry air at one atmosphere pressure and 500°F (260°C), a standard set of conditions.

The dimensionless heat transfer in a heat exchanger is measured by the exchanger effectiveness which in turn depends upon N_{tu} for fixed flow rates. In a "balanced" heat exchanger, the thermal resistances of both sides of a heat exchanger are of the same order of magnitude; hence N_{tu} is proportional to hA or $h_{std}A$. Thus, the higher h_{std} for a specified E_{std}, the lower is the heat-transfer area A requirement for the specified exchanger effectiveness; and as $A = \alpha V = (4p/D_h)V$, for a fixed D_h, the smaller is the heat exchanger volume for a given porosity, p.

As h_{std} is constant for fully developed laminar flow and does not vary with E_{std}, it is plotted against the aspect ratio α^* in Fig. 7 to cover the entire family of rectangular, trapezoidal, sine and isosceles triangular ducts. From this figure, it can be seen that h_{std} varies from 23·6 to 101·2 Btu/(h ft² °F) (a factor of 4·3); and $h_{std} = 38{\cdot}2$ Btu/(h ft² °F) for the equilateral triangular duct.* Thus the parallel plates heat exchanger would require 62 per cent (1–38·2/101·2) less heat-transfer area compared to the equilateral triangular heat exchanger. Additionally, if both the exchangers are designed for the same E_{std} and W, the parallel plate heat exchanger will also have 62 per cent less pressure drop. It should be pointed out that the effect of flow area and volume goodness factors is not necessarily cumulative. If the above advantages in A, V and Δp are to be realized simultaneously, the required free flow area for parallel plates will be larger. From equation (54),

$$A_c \propto \sqrt{\left(\frac{f}{j\Delta p}\right)}. \tag{55}$$

Hence, the parallel plates heat exchanger would require a 34 per cent $[\sqrt{\{1/(1{\cdot}47 \times 0{\cdot}377)\}} - 1]$ more free flow area, and for the same porosities, a 34 per cent more frontal area than the equilateral triangular matrix. However, for a common pressure drop (not the same E_{std}), the previous gain of the 18 per cent reduction in frontal area would still apply along with the 62 per cent reduction of volume for parallel plate heat exchanger for the same W, N_{tu} and p.

From the foregoing viewpoints, the rectangular duct family with $\alpha^* \leqslant 0{\cdot}25$ appears to be most promising from Figs. 6 and 7. However, the isosceles triangular or sine duct surfaces are more readily fabricated relative to $\alpha^* \leqslant 0{\cdot}25$ rectangular duct surfaces. A practical attempt to fabricate the latter surface for a regenerator is the so-called deepfold rectangular passage ($2b/2a = 8$) surface. Theoretically, it has $j_{H1}/f = 0{\cdot}359$ and $h_{std} = 79{\cdot}8$ Btu/(h ft² °F). However, if the passages of such a surface are of the trapezoidal shape with $\phi = 85°$ due to manufacturing process, instead of perfect rectangles, a severe degradation in the performance results. The equivalent trapezoidal duct having the same width at the middle of the channel has $2b/2a = 26{\cdot}7$ for $\phi = 85°$. This geometry has theoretical $j_{H1}/f = 0{\cdot}237$ and $h_{std} = 40{\cdot}0$ from Figs. 6 and 7. Thus, a 5° inclination in the long side of the rectangular duct results in a reduction of 34 and 50 per cent respectively in j_{H1}/f and h_{std} factors. In terms of heat-transfer area requirement, this means a penalty of 50 per cent. In reality, a 5° inclination may be excessive, but the results of Figs. 4–7 clearly demonstrate that the heat transfer and pressure drop of a deepfold surface may be very sensitive to the tooling used to form the passage geometry.

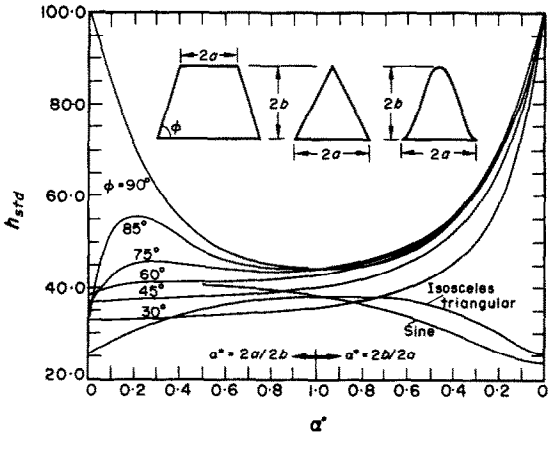

FIG. 7. Isosceles triangular, sine and trapezoidal ducts h_{std} for fully developed laminar flow (based on (H)).

*$Pr = 0{\cdot}680$; $\mu = 0{\cdot}06748$ lb$_m$/h ft; $c_p = 0{\cdot}2476$ Btu/lb$_m$ °F; $k = 0{\cdot}02458$ Btu/h ft °F; $\rho = 0{\cdot}04132$ lb$_m$/ft³.

*1 Btu/(h ft² °F) = 5·678 W/(m²K).

Influence of departure from idealized passage geometry

The passage geometry of an actual heat exchanger core can be significantly different from the idealized geometry. As mentioned in the Introduction Section, an equilateral triangular passage heat exchanger core often has passages of rounded corners and sine geometries. The theoretical performance of such a core can be significantly different from that of a core with ideal passages. The differences in heat transfer and pressure drop of such a "nonuniform" core may be assessed based on the method outlined by London [13].

Four "nonuniform" cores are considered as examples to illustrate the use of numerical results presented earlier and to bring out the effects of idealized non-uniformities: (1) equilateral triangular passage cores having (a) 50 per cent zero rounded corner and 50 per cent three rounded corner equilateral triangles and (b) 100 per cent three rounded corner equilateral

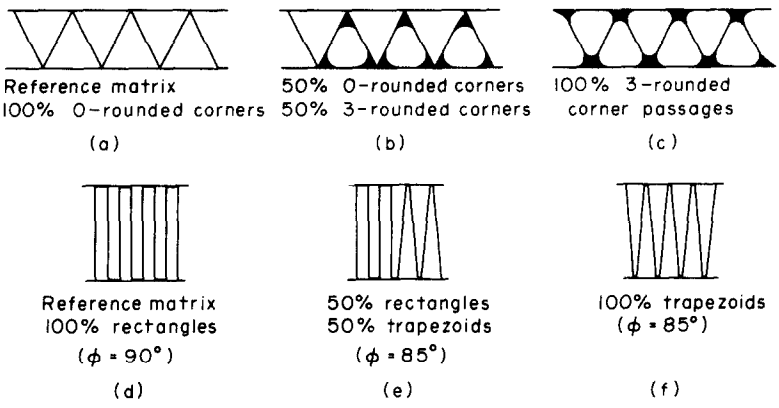

FIG. 8. Idealized uniform and nonuniform matrix passage geometries for the results of Table 7.

triangles; (2) 8 to 1 ($2b/2a = 8$) aspect ratio rectangular passage cores having (a) 50 per cent rectangles and 50 per cent trapezoidal passages with $\phi = 85°$ and (b) 100 per cent trapezoidal passages with $\phi = 85°$. The idealized uniform (reference cores) and nonuniform passage geometries are presented in Fig. 8. For each of the four cores of (1) and (2), the heat exchanger frontal area, flow length, and passage mid-wall thicknesses are specified to be the same as those for the reference cores.

The comparisons are made considering equal flow rates through the nonuniform and the appropriate uniform (reference) cores. The basic relations for N_{tu} and Δp of a heat exchanger employed are

$$N_{tu} = \frac{hA}{Wc_p} = \left(\frac{kL}{Wc_p}\right)\left(\frac{NuP}{D_h}\right) \tag{56}$$

$$\Delta p = f\frac{4L}{D_h}\frac{\rho u_m^2}{2g_c} = \left(\frac{2\mu LW}{g_c \rho}\right)\left(\frac{fRe}{A_c D_h^2}\right). \tag{57}$$

It is idealized that the flow is fully developed throughout the flow length and can be treated as at a constant density for the Δp evaluation. Moreover, μ, c_p, k, ρ and L are considered as constants. The ratios of effective N_{tu}, Δp and W of a nonuniform core to the appropriate reference core, designated as N_{tu}^*, Δp^* and W^*, are presented in Table 7. The method of London [13] is used to determine N_{tu} of the nonuniform cores which in turn depends upon N_{tu} of the reference cores.

Table 7. Influence of rounding of corners on an equilateral triangular matrix and of trapezoidal passages in a deepfold rectangular matrix

	Equilateral triangular		Deepfold rectangular	
	geometry of Fig. 8(b)	geometry of Fig. 8(c)	geometry of Fig. 8(e)	geometry of Fig. 8(f)
W^*	1	1	1	1
Δp^*	1·044	1·092	0·867	0·766
N_{tu}^*	0·964*	0·927	0·616†	0·505

*Even though N_{tu}^* depends on $N_{tu,ref}$, N_{tu}^* is 0·964 for $1 \leqslant N_{tu,ref} \leqslant 20$.

†The magnitude of N_{tu}^* is 0·686, 0·635, 0·623 and 0·616 for the values of $N_{tu,ref}$ as 1, 5, 10 and 20 respectively.

A review of the results of Table 7 reveals that the rounding of corners of a triangular matrix has only a small adverse influence on the N_{tu} and Δp of the core. In contrast, a severe degradation in N_{tu} results for a deepfold surface having all trapezoidal section passages with $\phi = 85°$. From Table 7, a 49·5 per cent (1 − 0·505) reduction (degradation) results in N_{tu} compensated in part by a 23·4 per cent (1 − 0·766) reduction in pressure drop for the Fig. 8(f) geometry.

CONCLUSIONS

A least-squares-matching method is presented to analyze fully developed laminar flow and forced convection heat transfer in ducts under axially constant wall heat flux and peripherally arbitrary thermal boundary conditions. As an application of the method, numerical results are provided in Tables 1–6 for the isosceles triangular, rounded corner equilateral triangular, sine, rhombic, trapezoidal and rectangular ducts. The influence of passage geometry on the heat exchanger design is shown in Figs. 6 and 7 in terms of flow area and volume goodness factors. It is shown that the rounding of corners of an equilateral triangular matrix has only a small effect on the heat exchanger performance. In contrast, if a deepfold passage geometry ($2b/2a = 8$) has all trapezoidal passages, a very significant reduction in the heat exchanger performance occurs relative to true rectangular passages.

Acknowledgements—This work was started under the Office of Naval Research Contract Nonr 225(91), NR-090-342 at Stanford University. The author is grateful to Prof. A. L. London for his guidance and encouragement, and to R. Noyes of General Motors Technical Center for providing a computer program based on Sparrow and Haji-Sheikh's method.

REFERENCES

1. R. K. Shah and A. L. London, *Laminar Flow Forced Convection Heat Transfer*. Academic Press, New York. To be published.
2. E. M. Sparrow and A. Haji-Sheikh, Flow and heat transfer in ducts of arbitrary shape with arbitrary thermal boundary conditions, *J. Heat Transfer* **88C**, 351–358 (1966).

3. G. H. Golub, Numerical methods for solving linear least-squares problem, *Num. Math.* **7**, 206–216 (1965).
4. A. Ralston, *A First Course in Numerical Analysis.* McGraw-Hill, New York (1965).
5. R. K. Shah, Laminar flow forced convection heat transfer and flow friction in straight and curved ducts—a summary of analytical solutions, Ph.D. Thesis, Mech. Engrg. Dept., Stanford University, Stanford, California (1972).
6. F. W. Schmidt and M. E. Newell, Heat transfer in fully developed laminar flow through rectangular and isosceles triangular ducts, *Int. J. Heat Mass Transfer* **10**, 1121–1123 (1967).
7. D. F. Sherony and C. W. Solbrig, Analytical investigation of heat or mass transfer and friction factors in a corrugated duct heat or mass exchanger, *Int. J. Heat Mass Transfer* **13**, 145–159 (1970).
8. E. M. Sparrow and A. Haji-Sheikh, Laminar heat transfer and pressure drop in isosceles triangular, right triangular and circular sector ducts, *J. Heat Transfer* **87C**, 426–427 (1965).
9. M. Iqbal, B. D. Aggarwala and A. G. Fowler, Laminar combined free and forced convection in vertical noncircular ducts under uniform heat flux, *Int. J. Heat Mass Transfer* **12**, 1123–1139 (1969).
10. K. C. Cheng, Laminar forced convection in regular polygonal ducts with uniform peripheral heat flux, *J. Heat Transfer* **91C**, 156–157 (1969).
11. M. Iqbal, A. K. Khatry and B. D. Aggarwala, On the second fundamental problem of combined free and forced convection through vertical noncircular ducts, *Appl. Scient. Res.* **26**, 183–208 (1972).
12. R. H. Bartels and G. H. Golub, Stable numerical methods for obtaining the Chebyshev solution to an overdetermined system of equations, *Communications of the ACM* **11**(6), 401–406, 428–430 (1968).
13. A. L. London, Laminar flow gas turbine regenerators—the influence of manufacturing tolerances, *J. Engng Pwr* **92A**, 46–56 (1970).

APPENDIX

Householder Reflection

An $m \times m$ square matrix $\mathbf{P}$ of the following form is called a Householder reflection

$$\mathbf{P} = \mathbf{I} - \frac{1}{\beta}\mathbf{v}\mathbf{v}^T \tag{58}$$

where $\mathbf{I}$ is an identity matrix and

$$\beta = \tfrac{1}{2}\|\mathbf{v}\|^2 = \mathbf{v}^T\mathbf{v}/2 \tag{59}$$

for any vector $\mathbf{v} = (v_1, \ldots, v_n)^T$. It can be readily proved that the Householder reflection $\mathbf{P}$ is its own inverse and its own transpose and hence it is orthogonal.

The important property of the Householder reflection is that for any nonzero vector $\mathbf{g}$, it is possible to find a Householder reflection $\mathbf{P}$ which annihilates the desired elements of this vector. Consider one wants to keep $g_1, \ldots, g_{j-1}$ unchanged, change g_j, and make $g_{j+1}, \ldots, g_m$ as zero. In that case, define

$$\alpha = \text{sign}\,(g_j)\,(g_j^2 + g_{j+1}^2 + \ldots + g_m^2)^{1/2} \tag{60}$$

$$\mathbf{v} = (0, \ldots, 0, g_j + \alpha, g_{j+1}, \ldots, g_m)^T \tag{61}$$

$$\beta = \alpha(g_j + \alpha) \tag{62}$$

where sign (g_j) is 1 if $g_j > 0$ and -1 if $g_j < 0$. Substituting equations (60), (61) and (62) into equation (58) provides the Householder reflection $\mathbf{P}_j$ which when operated on $\mathbf{g}$ yields the desired vector.

$$\mathbf{P}_j\mathbf{g} = (g_1, \ldots, g_{j-1}, -\alpha, 0, \ldots, 0)^T. \tag{63}$$

Furthermore, if $\mathbf{h}$ is any vector with not all h_1 through h_{j-1} as zero and h_j through h_m as zero, then $\mathbf{P}_j$ yields the vector

$$\mathbf{P}_j\mathbf{h} = \mathbf{h}. \tag{64}$$

However, if all the elements h_j through h_m are not zero, define a constant γ as

$$\gamma = (v^T h)/\beta, \tag{65}$$

then

$$\mathbf{P}_j\mathbf{h} = \mathbf{h} - \gamma\mathbf{v}. \tag{66}$$

The aforementioned property of the Householder reflection is employed to reduce the system of equation (1) into the upper triangular system of equation (3). For the Householder reflection $\mathbf{P}_1$, the vector $\mathbf{g}$ is considered as the first column of matrix $\mathbf{A}$. α, $\mathbf{v}$, β and γ are computed by equations (60), (61), (62) and (65) with $j = 1$. The application of $\mathbf{P}_1$ on the first column of $\mathbf{A}$ results in its first element as $-\alpha$ and the rest as zero. The second through nth column and $\mathbf{P}_1\mathbf{v}$ are obtained by use of equation (66). The successive application of $\mathbf{P}_2, \ldots, \mathbf{P}_n$ results in the matrix equation (3). To minimize the roundoff errors in the numerical computation, at each step a pivoting is done by choosing the column with the largest sum of squares of matrix $\mathbf{A}$ to be reduced next.

It should be emphasized that the application of the Householder reflection $\mathbf{P}$ does not mean the matrix multiplication, but it means obtaining the r.h.s. of equations (60), (61) and (63) which at the most involves the vector inner product and vector subtraction.

FROTTEMENT ET TRANSFERT DE CHALEUR EN CONVECTION FORCEE LAMINAIRE DANS LES CONDUITES A GEOMETRIE ARBITRAIRE

Résumé—Une méthode d'optimisation au sens des moindres carrés est présentée afin d'analyser l'écoulement laminaire établi et le transfert de chaleur dans les conduites de section arbitraire. Le transfert thermique en convection forcée est considéré dans le cas d'un flux longitudinalement constant avec des conditions aux limites thermiques arbitraires sur la périphérie. A titre d'application de la méthode, des résultats dynamiques et thermiques sont présentés pour des géométries de conduites à section droite comprenant, des triangles isocèles, triangles équilatéraux à sommets arrondis, sinus, losanges et trapèzes.

Ces résultats numériques sont discutés en vue de la conception des échangeurs de chaleur.

LAMINARER REIBUNGS-DRUCKABFALL UND WÄRMEÜBERGANG BEI ERZWUNGENER KONVEKTION IN KANÄLEN BELIEBIGER GEOMETRIE

Zusammenfassung—Zur Untersuchung der vollausgebildeten Laminarströmung und des Wärmeübergangs in Kanälen beliebigen Querschnitts wird eine Methode der kleinsten Fehlerquadrate vorgestellt. Der Wärmeübergang bei erzwungener Konvektion wird unter der Voraussetzung konstanten axialen Wärmedurchsatzes bei beliebigen thermischen Randbedingungen an der Berandung behandelt. Als Anwendungs-

beispiel des Verfahrens werden Lösungen für Strömung und Wärmeübergang für folgende Kanalquerschnitte vorgestellt: gleichseitig dreieckig, gleichseitig dreieckig mit abgerundeten Ecken, sinusförmig, rhombisch und trapezförmig. Diese numerischen Ergebnisse werden aus der Sicht des Wärmeübertragerkonstrukteurs diskutiert.

ТРЕНИЕ И ПЕРЕНОС ТЕПЛА ПРИ ЛАМИНАРНОЙ ВЫНУЖДЕННОЙ КОНВЕКЦИИ В ТРУБАХ ПРОИЗВОЛЬНОЙ ФОРМЫ

Аннотация — В статье рассматривается применение метода наименьших квадратов для исследования полностью развитого ламинарного течения жидкости и теплообмена в трубах произвольного сечения. Теплоперенос при вынужденной конвекции рассматривается при постоянном осевом тепловом потоке и произвольных периферических тепловых граничных условиях.

В качестве примеров представлены результаты по трению и теплообмену для сечений трубы в форме равнобедренного треугольника, равностороннего треугольника с закругленными углами, а также синусоидального, ромбического и трапецеидального сечений. Полученные численные результаты рассматриваются с точки зрения конструирования теплообменников.